Dielectrophoretically Modulated Optical Spectroscopy of Colloidal Nanoparticle Solutions in Microfluidic Channels

Clyde Midelet, Martinus H. V. Werts

Dielectrophoretically modulated optical spectroscopy of colloidal nanoparticle solutions in microfluidic channels

Clyde Midelet[a,b] *and Martinus H. V. Werts*[a,b]*

[a] Dr. Clyde Midelet, Dr. Martinus H. V. Werts
Univ Rennes, CNRS, SATIE - UMR 8029, F-35000 Rennes, France

[b] Dr. Clyde Midelet, Dr. Martinus H. V. Werts
École normale supérieure de Rennes, SATIE, Av. R. Schuman, Campus de Ker Lann, F-35170 Bruz, France

E-mail : martinus.werts@ens-rennes.fr

Keywords: dielectrophoresis; gold nanoparticles; optical spectroscopy; microfluidics; nanomanipulation

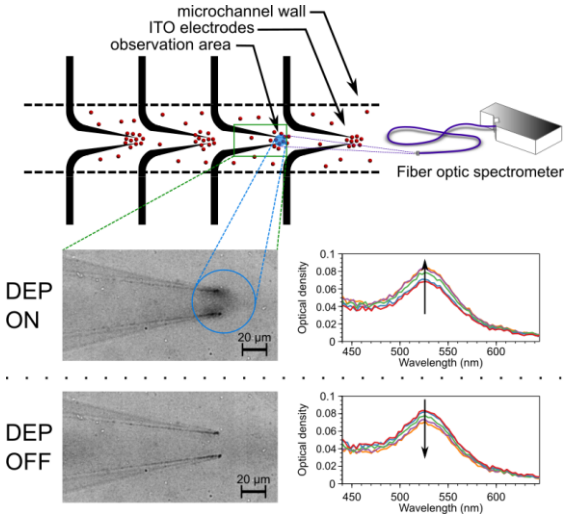

Catch & release. *Periodic trapping of colloidal nanoparticles by dielectrophoresis (DEP) in a microfluidic system is the basis of DEP-modulated optical spectroscopy. This technique is demonstrated to be useful for the measurement of the electric polarizabilities of sub-100 nm gold nanoparticles and for disentangling the extinction spectra of multicomponent mixtures.*

Abstract

Optical spectroscopic techniques (*e.g.*, extinction, scattering and fluorescence spectroscopies) are important for the analysis of colloidal solutions of nanoparticles (NPs). They are routinely applied to plasmonic and quantum-dot NP samples assuming that these contain a single population of particles with modest size and shape dispersity. However, these spectroscopic techniques become less effective when the sample is a mixture of particles with different sizes, shapes or composition. Here, we propose an original microfluidic method for the optical spectroscopic analysis of colloidal NP solutions that combines periodic trapping of NPs by dielectrophoresis (DEP) with *in situ* optical extinction spectroscopy. The periodic trapping leads to modulation of the continuously monitored optical spectrum depending on the DEP properties of the NPs. DEP-modulated spectroscopy is demonstrated using colloidal gold NPs as small as 40 nm diameter. It is found that the DEP modulation is significantly enhanced when employing suitable microfluidic flow over a multi-electrode array. Finally, we show that the method can identify and characterize the NP species simultaneously present in a mixture of 40 nm and 80 nm gold NPs, opening the way towards optical spectroscopic analysis of higher complexity NP mixtures through the combination of the DEP-modulated spectroscopy with chemometric methods.

1. Introduction

Steady-state optical spectroscopic techniques are instrumental to the analysis of colloidal solutions of synthetic and natural nanoparticles (NPs). For instance, optical extinction spectroscopy (also referred to as UV-visible absorbance spectrometry) is routinely used as a characterization method for molecules and NPs in solution. The measurements are typically

done on bulk solutions at equilibrium, and yield one single extinction spectrum for a sample. In the case of a single detectable chemical species present in the solution (*e.g.* a perfect solution of a pure substance in a liquid), this single spectrum is representative for the optical spectroscopic response of the species in solution. In the case of a mixture of (spectroscopically detectable) species, information on the spectroscopic response of the individual species cannot be directly derived from a single spectrum without additional information. Moreover, without any further analytical data (*e.g.* chromatography, reference spectra), it is not possible to tell from a single spectrum if it corresponds to a single species or to a mixture.

Instead of measuring a single spectrum of the sample at equilibrium, a series of spectra may be recorded while perturbing the sample using an external stimulus. In that case, the perturbation may lead to measurable variations over the recorded series of optical spectra. These variations are connected to the perturbation through a (potentially long) chain of physical and chemical phenomena. In an ideal case, analysis of the fluctuations of the spectra will provide spectroscopic information on each of the (spectroscopically active) chemical species in the sample and give access to those physico-chemical properties of the sample that impart sensitivity towards the external stimuli used for the perturbation.

In the context of measurement of optical spectra of samples subject to external perturbations, mention can be made of the stopped-flow technique,[1,2] in which rapid mixing of reactants leads to a sample in a non-equilibrium state whose evolution towards equilibrium is monitored with optical spectroscopy. Flash photolysis,[3,4] another technique, studies the evolution of the optical (absorption) spectrum upon perturbation of the sample by a flash ('delta pulse') of light. A related method is photoinduced absorption (PIA) spectroscopy,[5] in which the sample is perturbed by a periodic (optically chopped laser) excitation. Also, microfluidics has been used to study photoinduced chemical reactions on the microsecond scale, using fluorescence

detection of the products.[6] Microfluidics coupled to Raman microscopy has been used to measure diffusion coefficients in binary solvent systems.[7]

Here, we propose to measure optical extinction spectra of liquid solutions of colloidal NPs inside microfluidic channels while using *in-situ* microscale dielectrophoresis (DEP) as a perturbation. The dielectrophoretic field is generated by tip-shaped thin-film microelectrodes[8,9] and is periodically switched "ON" and "OFF" on regular intervals, leading to periodic trapping of NPs. This leads to a measurable modulation in the optical extinction spectra, due to DEP-induced variations in the concentrations of the NPs. When the field is switched on, the NPs are locally concentrated on the tips of the microelectrodes. This local concentrate subsequently dissipates as a result of free diffusion after switching the field off. Different types of NPs are expected to respond differently to the applied DEP field.

DEP is the directed motion of small polarizable particles suspended in a fluid due to an electric field with strong gradients.[10–12] It has been used in microfluidics to manipulate bioparticles (cells, viruses),[13–15] and can also be applied to NPs and biomolecules such as proteins and DNA.[16–22] Microfluidic systems, dielectrophoresis and optical detection may be combined together.[23–26] Dielectrophoretic particle collection has been measured using transmitted light measurement with an LED-photodiode combination.[27] DEP particle focussing has been combined with confocal optical detection,[28] and DEP has been combined with Raman spectroscopy.[29] In the latter case, the DEP serves to concentrate NPs prior to spectroscopy. Application of a dielectrophoretic perturbation to DLS measurements has also been investigated.[30] Thus far, however, DEP has not been applied to the modulation of optical extinction spectra. The periodic modulation of local concentrations by DEP presented here may be used with other spectroscopic techniques, *e.g.* fluorescence emission spectroscopy or Raman spectroscopy, by modifying the configuration of the microscope.

The present work was initially motivated by our desire to measure the dielectrophoretic susceptibility of gold NPs smaller than 80 nm. In a recent study,[9] we measured the dielectrophoretic response of sub-200 nm gold spheres in a microfluidic system using side-illuminated dark-field video-microscopy. Gold NPs smaller than 80 nm were not accessible in this method due to the weak light scattering by such small particles. Here, we report that sub-80 nm gold NPs are indeed accessible using DEP-modulated optical extinction spectroscopy, which detects the absorption of light by NPs in addition to light losses through scattering. Interestingly, we established that DEP-modulated optical spectroscopy can serve as a microscale *in-situ* separation method that can help in rapidly identifying different sub-populations in a small-volume sample by generating time-dependent spectra containing varying contributions of each of the sub-populations. Such multivariate spectrotemporal data are amenable to chemometric analysis that can extract the spectral responses of several sub-populations present in a mixture.[31,32]

The DEP-modulated spectroscopy described in this paper is illustrated in Figure 1. It employs a device consisting of a microfluidic channel engraved in an elastomer positioned on top of a substrate of fused silica. The substrate carries an array of sharply-tipped thin-film electrode pairs. These electrodes produce the DEP field upon application of an electric potential difference. The microfluidic channel is filled with aqueous samples containing colloidal NPs. A periodic perturbation is applied, repeatedly switching ON and OFF the dielectrophoretic field while continuously recording optical extinction spectra of the microscopic volume using a fibre-coupled CCD-array spectrometer.

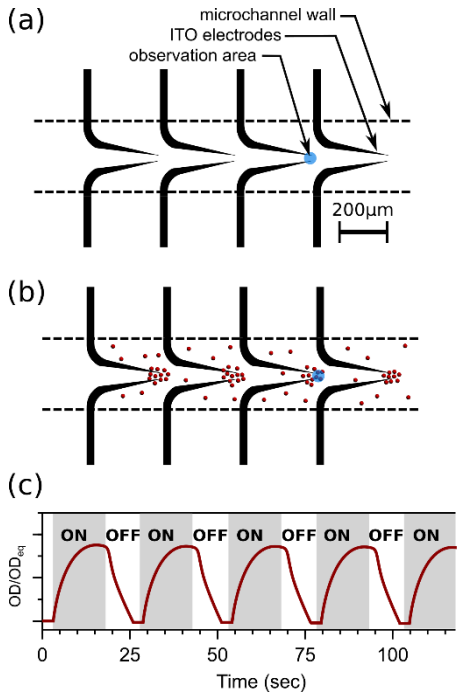

Figure 1. (a) Schematic top-view of the microfluidic channel showing the relative sizes of electrodes and the capture area sampled by the spectrophotometer (actual diameter 51 µm, see Supporting Information S1). Dashed lines correspond to edges of the microchannel. (b) DEP capture of particles near the tips of the electrodes along the microelectrode array. (c) Expected periodic modulation in the optical density at a single wavelength as a result of periodic dielectrophoresis.

The optical extinction spectra in the recorded sequence display periodic changes due to changes of the local concentrations of NPs in the observation volume reflecting the periodic capture and release by DEP. The specific time-evolution of the concentration of each type of particle in the sample depends on its DEP mobility,[33,34] and its Fickian diffusion coefficient. For a given type of colloidal system, the DEP mobility depends strongly on the size of the NP. In this work, we use DEP-modulated optical extinction spectroscopy to extend our prior measurements of the size-dependence of dielectrophoresis for gold NPs smaller than 100 nm. Furthermore, we demonstrate the feasibility of detecting and spectroscopically characterizing two populations of different particles simultaneously present in a sample.

2. Results and discussion

2.1. Extinction spectroscopy in the microfluidic cell

A CCD-array spectrometer was coupled to the microscope side port via an optical fibre and used to record spectra of the collected light corresponding to a circular area of the microscope image. The microscope objective had a magnification of 20 x (NA 0.4). The optics were set up in such a way that the sampled area had a diameter of 50 μm **(**see Supporting Information, section S1**)**. The recorded spectra are thus averages over the volume covered by this area. A relatively large area was chosen in order to increase stability and signal-to-noise ratio of the measurement. The optical pathlength through the sample (*i.e.* the microchannel height) is 20 μm, giving a sampled volume of 40 pL.

Spectra of injected pure water solvent and of gold NPs in aqueous solution were recorded (see Supporting Information, section S2). The pure-solvent baseline spectrum is sufficiently stable over several tens of minutes to reliably measure extinction spectra of the solution in the microfluidic volume. The spectra recorded for concentrated gold NP solutions (see Experimental Section) correspond well to the expectations on basis of spectra recorded in a traditional cuvette taking into account the concentration factor and the optical path length. For instance, the spectrum of an aqueous solution of Au40-LA NPs (40 nm diameter gold NPs, 3.20 x 10^{-9} mol L^{-1}) shows the expected plasmon resonance extinction band. Its optical density corresponds well to the density expected for the 20 μm pathlength (nominal OD_{1cm} = 25, expected for 20 μm: 0.050, found: $OD_{20\mu m}$ = 0.058).

2.2. DEP-modulation of extinction spectra in the absence of microfluidic flow

First, we studied DEP-modulated extinction spectroscopy for a series of differently sized gold nanospheres Au40-LA, Au80-LA and Au100-LA (40, 80 and 100 nm diameter, respectively; see Experimental section) inside the channel in absence of microfluidic flow. Electrohydrodynamic phenomena[35–38] were avoided by using an AC electric field at a frequency of 1 MHz and an applied amplitude of 20 V_{pp}.[9] After injection of the liquid sample, the microflow was stopped using the pressure-driven flow controller and dielectrophoretic modulation was started. In a typical experiment, the cycle period was composed of 15 seconds of dielectrophoretic capture ("DEP ON") to let enough time for a sufficient number of particles to be captured. This was followed by 10 seconds of release ("DEP OFF") during which the NPs diffuse freely. This DEP cycle was repeated indefinitely. Once a steady modulation of the optical spectra was reached (typically, after 10 cycles), extinction spectra were recorded over time. Figure 2 shows a typical result for Au40-LA NPs.

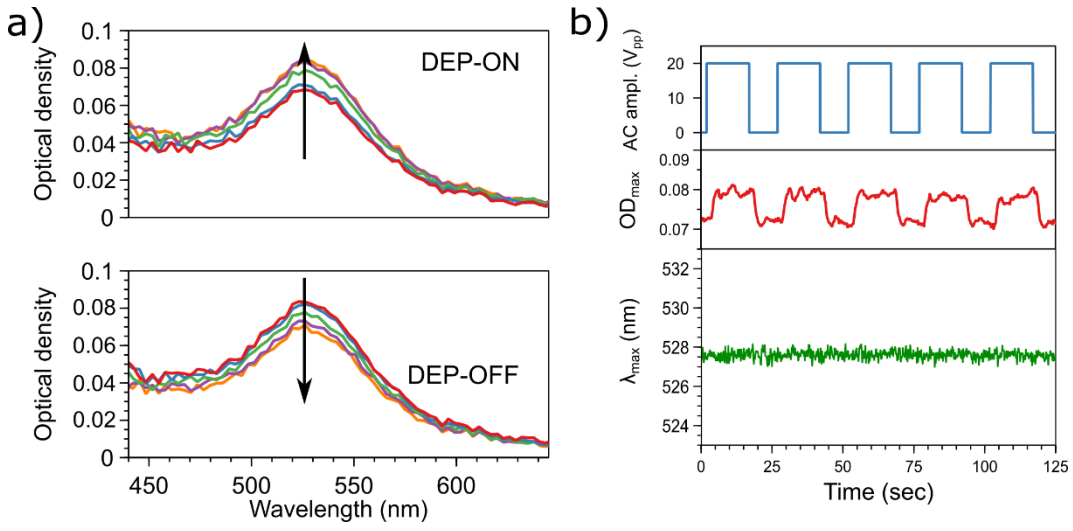

Figure 2. DEP-modulated optical extinction spectroscopy of Au40-LA in aqueous solution. (a) Evolution of the extinction spectrum in the observation volume; *top*: during the "DEP ON" phase; *bottom*: during the "DEP OFF" phase. (b) *top*: Amplitude of the applied AC potential for DEP; *middle*: evolution of the measured optical density at λ_{max} as a function of time; *bottom*: position of the maximum of the extinction band (λ_{max}) as a function of time, showing the absence of wavelength shifts.

The intensity of the extinction band corresponding to the Au40-LA plasmon resonance is modulated as the DEP field is switched "ON" and "OFF". The optical density increases as the field is switched on, indicating an increase of the number of particles in the observation volume. When the DEP field is switched off the extinction drops rapidly to its equilibrium value. This drop corresponds to the rapid free diffusion after release of the NPs from the electrode tips. There is a slight phase delay between the switching of the DEP field and the observed optical response, indicative of the limited rate of DEP capture and free NP diffusion. Importantly, the periodic modulation using DEP can be maintained over prolonged periods without noticeable changes to the extinction spectra of the sample, demonstrating that it remains intact.

Further analysis of the set of the DEP-modulated spectra of the single-component Au40-LA sample shows that the modulation only affects the intensity of the spectral bands, but not their shapes. This is illustrated by the plot of the wavelength of the maximum of the extinction band as a function of time in Figure 2b. The position of the maximum is entirely unaffected by the DEP modulation, whereas its height is indeed modulated. This indicates that DEP does not induce aggregation of the nanoparticles. Aggregation would lead to changes in the spectra, depending on the inter-particle distance in the aggregates.[39]

The absence of aggregation is in part due to the high colloidal stability of LA-coated nanoparticles, which at the basic pH employed bear negatively charged carboxylate groups. More importantly, the concentration increase by DEP in our device is rather modest, at most a factor of 2 in the present work. For Au40-LA particles the local nanoparticle concentration then increases from 3.2 nM to 6.4 nM (1.9×10^{12} NPs mL^{-1} to 3.8×10^{12} NPs mL^{-1}). The average interparticle distance in the solution thus decreases from 0.8 μm to 0.6 μm. This explains the lack of wavelength shifts due to plasmon coupling. For samples of larger particles, the

concentrations are even lower, and the interparticle distances larger. We previously studied the DEP trapping process of the same type of gold NPs near the electrodes using dark-field videomicroscopy.[9] From these studies, we find that the factor of DEP-induced concentration increase is always below 10, even at the very tip of the electrodes. Also, the DEP process was found to be completely reversible.

Measurements of DEP-modulated extinction spectra for 40, 80 and 100 nm gold NPs (Au40-LA, Au80-LA, Au100-LA) were performed using identical experimental settings. The periodically DEP-modulated spectra were recorded for a prolonged time (5 min.). The modulation was verified to be stable over this duration and no changes to the shape of the spectra were observed; only the height of the spectra changed. Plots of typical DEP modulation cycles (in terms of optical density at the wavelength of the extinction maximum as a function of time) can be found in the Supporting Information, section S3.

The modulated optical densities are analysed in terms of the factor by which the optical density increases as a result of dielectrophoretic concentration of NPs relative to the optical density at equilibrium. We call this *capture factor* ψ_{cap}. It is closely related to the *capture ratio* Φ_{cap} that we used in our prior work: $\psi_{cap} = \Phi_{cap} - 1$.[9] The capture factor is obtained as the ratio of the peak-to-valley amplitude of the modulation of the optical density ($OD_{max} - OD_{min}$) and its equilibrium value (OD_{eq}). The optical densities were taken at the wavelengths λ_{max} where the NPs' plasmonic extinction bands have their maximum.

$$\psi_{cap} = \frac{OD_{max} - OD_{min}}{OD_{eq}} \qquad (1)$$

The capture factor ψ_{cap} is 0 if no capture takes place, and becomes greater as more particles are captured during the "DEP on" phase. It is proportional to the average dielectrophoretic force

experienced $\langle \mathbf{F}_{\mathrm{DEP}} \rangle$ by the particles. Following Eqn. (2), this force depends on the dielectrophoretic susceptibility of the nanoparticle (K_{pol}), and on the amplitude of the applied AC potential (scalar U) and the topology of the electric field (normalized vector field **G**).[9] The electric field is given in this expression by $\mathbf{E} = \mathrm{U}\mathbf{G}$.

$$\langle \mathbf{F}_{\mathrm{DEP}} \rangle = \frac{1}{4} \mathrm{K}_{\mathrm{pol}} \mathrm{U}^2 \nabla |\mathbf{G}|^2 \qquad (2)$$

For a series of different NPs measured using constant parameters of the applied electric field (amplitude, frequency, topology), the capture factors ψ_{cap} are proportional to the dielectrophoretic susceptibilities K_{pol} of the particles. Therefore, we measured ψ_{cap} for a series of particles with different diameters using constant experimental settings. For a single measurement on each particle diameter, the capture factors were averaged over several DEP cycles (typically 10 cycles per measurement). The experimental capture factors for NPs of varying diameter are collected in Table 1.

Table 1. Wavelength of the extinction maximum and DEP capture factor ψ_{cap} (95% confidence intervals) obtained using DEP-modulated optical extinction spectroscopy for gold NPs of different diameters in aqueous solution. Applied AC electric field had an amplitude of 20 V_{pp} and a frequency of 1 MHz.

	λ_{max} (nm)	ψ_{cap}
Au40-LA	528	0.20 (±0.11)
Au80-LA	549	0.35 (±0.13)
Au100-LA	572	0.44 (±0.15)

The capture factor increases as the NP diameter increases, indicating as expected that larger particles are more susceptible to dielectrophoresis, displaying a larger relative dielectrophoretic susceptibility K_{pol}. By taking the ratio of ψ_{cap} for two different diameters of particles, the ratio of $\mathrm{K}_{\mathrm{pol}}$ for these particles is obtained. From the present set of measurement this yields a series

of relative DEP susceptibilities. In our previous work, we determined relative DEP susceptibilities for 80, 100 and 150 nm gold NPs using dark-field video-microscopy.[9] Smaller particles did not generate sufficient contrast in that technique. Here, we obtain results for 40, 80, 100 nm gold NPs with DEP-modulated extinction spectroscopy. The overlap between the two types of measurement enables to compare, combine and extend the results (Figure 3).

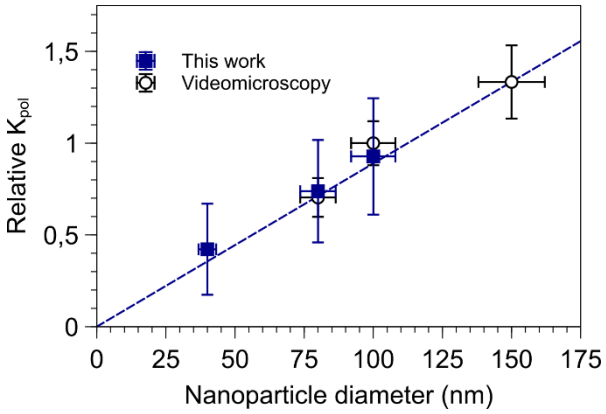

Figure 3. Combined results for the relative dielectrophoretic susceptibilities K_{pol} as a function of diameter for spherical gold NPs in aqueous solution (0.2mM NaLA, 1mM NaOH). Unfilled circle markers indicate the results from dark-field video-microscopy;[9] filled squares are the result obtained in the present work using DEP-modulated spectroscopy. The dotted line suggests a linear dependence of dielectrophoretic susceptibility on nanosphere diameter.

The new results obtained using the DEP-modulated spectroscopy presented here further extend our observation,[9] that the relative dielectrophoretic susceptibility (and the DEP force for a given amplitude and frequency for the applied field) has a linear dependence on NP diameter for sub-200 nm gold particles, instead of the cubic dependence found for spheres with diameters larger than 1 μm. This means that the electric polarizability of sub-200 nm gold nanoparticles is larger than expected on basis of the classic dependence of the polarizability on particle volume. This is in line with recent findings obtained using DEP and fluorescence microscopy for 20 nm diameter quantum dots in water at low medium conductivity.[40]

2.3. Enhancement of DEP modulation using microfluidic flow

It was anticipated that a steady microfluidic flow of the NP solution over the array of electrode pairs in combination with periodic DEP may amplify the concentration of NPs by DEP. By carefully tuning the flow rate, DEP capture of NPs over the electrode array may be amplified as the advected particle "blobs" are increasingly concentrated at each electrode pair (see Supporting Information, section S4). The flow rate was adjusted so as to let enough time for particles to be recaptured at each pair of electrode tips during DEP (there is a pair every 300 µm along the channel), while ensuring that they are advected just from one electrode pair to the next during the phase that the DEP is inactive.

Figure 4 shows that microfluidic flow indeed enhances the overall yield of dielectrophoretic capture. Compared to DEP without flow, microfluidic flow was found to enhance the capture ratio by factors 1.1 (10%), 2.3 (130%) and 2.6 (160%), for 40, 80 and 100 nm diameter gold NPs, respectively.

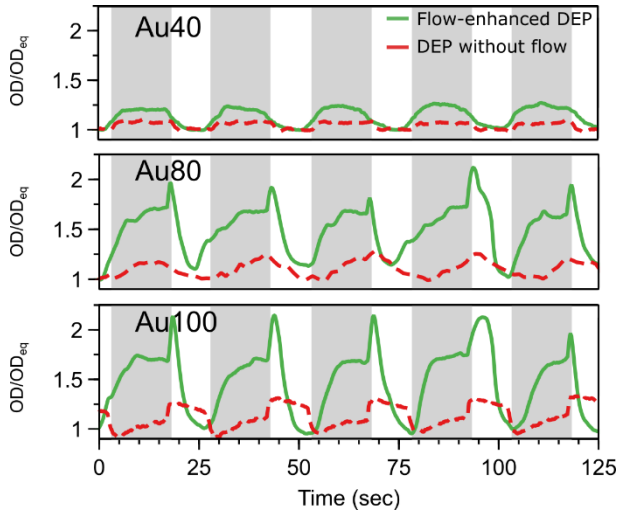

Figure 4. Flow-enhancement of DEP modulation for Au40-LA, Au80-LA and Au100-LA. The green solid lines are the DEP modulation cycles (relative optical density at wavelength of the extinction maximum) in presence of optimized microfluidic flow (avg. flow speed: 30 µm s^{-1}, see Section S4). The grey areas in the background show when the DEP field was switched on. For comparison, the graphs also contain the modulation curves in absence of flow (red dashed lines).

The higher enhancement observed for larger diameter particles can be attributed to the slower diffusion of the particles during the "DEP OFF" cycle, leading to less spreading out of the concentrated particle flocks as they are advected towards the next electrode pair. We expect the precise enhancement factor to depend simultaneously on electrode pair separation, dielectrophoretic force (which depends to the size of the particle here), NP diffusion coefficient, and flow velocity profile (which depends in turn on flow rate and channel geometry). Furthermore, the exact position of the observation volume relative to the capture zone will also be of influence. This will be further investigated in the future using numerical simulation of NP transport in this system. Measurements for quantitative determination of the DEP susceptibility of a given NP type (as described in Section 2.2) need therefore be done without flow, whereas measurements relying on maximum modulation by DEP but not requiring quantitative determination of DEP susceptibility will be improved using flow enhancement. This latter case concerns analytical applications such as multicomponent analysis.

2.4. Analysis of a two-component nanoparticle mixture

In this last part, the feasibility of multi-component analysis using (flow-enhanced) DEP-modulated extinction micro-spectroscopy is demonstrated. An aqueous solution containing a mixture of Au40-LA and Au80-LA particles was used for this. The concentration of each component in the mixture was chosen such that both components contribute approximately equally to the total optical density (see Supporting Information, section S5).

Like elsewhere in this work, an AC electric potential of 1 MHz, 20 V_{pp} was applied to the electrodes, with the DEP field being active for 15 seconds ("ON") and inactive for 10 seconds

("OFF"). As indicated above, the "on" time was chosen to optimize the signal (the longer the DEP, the higher the modulation). The "off" time was set to allow for sufficient diffusion after release to reach the equilibrium concentration again. Furthermore, for this flow-enhanced measurement, the duration of one DEP cycle period must be compatible with the microfluidic flow rate, as detailed in the previous section. Microfluidic flow was set up inside the microchannel using the pressure controller so as to enhance the dielectrophoretic capture of particles applying a flow speed of 30 μm s^{-1}.

The position of the observation volume was slightly shifted downstream compared to the other measurements in order to optimize the contrast between the DEP-modulated spectra of the 40 nm and the 80 nm NPs. Spectra were continuously recorded with the spectrophotometer using an exposure time of 250 milliseconds per spectrum, recording 4 spectra per second. A video, included with the Supporting Information (section S6 for a description), further illustrates the recording of optical spectra under flow-enhanced DEP modulation by showing simultaneously the images from the microchannel and the corresponding optical spectra. The DEP-modulated extinction spectra as a function of time are stored in a spectrotemporal matrix. A typical spectrotemporal matrix is shown in Figure 5.

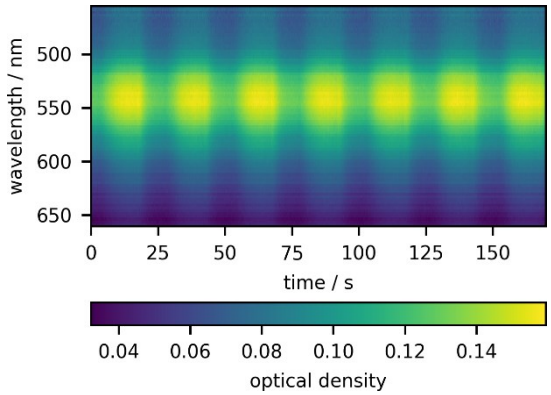

Figure 5. Series of DEP-modulated extinction spectra as a function of time for an aqueous solution of a mixture 1:1 of Au40-LA and Au80-LA represented in a spectrotemporal matrix plotted as a "heat map". The Supporting Information (description in section S6) includes a video showing simultaneously the images from the microfluidic device and the corresponding optical extinction spectra.

Inspection of the spectra in the experimental data shows that the maximum of the extinction spectrum shifts back and forth in response to the DEP modulation (Figure 6b), in contrast to the DEP-modulated extinction spectra of the single-component samples, which did not display such shifts (Figure 2b). The extinction spectra of pure Au40-LA and pure Au80-LA have their maxima at different wavelengths (528 nm *vs* 549 nm), but the extinction bands are broad and show significant overlap. As a result, the position of the extinction maximum will shift when the two components are mixed in different proportions. The observed DEP-modulation of the position of the maximum of the spectra of the mixture can be interpreted by the changes in relative concentrations of the two components, as will be shown now.

A straightforward approach was used to analyse the DEP-modulated spectra of the solution containing the mixture of Au40-LA and Au80-LA NPs. The known spectra of the components (see Supporting information, section S5) were used to obtain the relative concentrations at each time-step during the DEP cycle by fitting the concentration coefficients such that the weighted sum of the spectra reproduces the observed spectrum. The coefficients were found via a least-squares fitting procedure using the Nelder-Mead algorithm for optimization.[41,42] The fit coefficients are proportional to the (relative) concentrations of the individual components, hence plotting them as a function of time yields a graph of the evolution of the relative concentrations of the components over time (Figure 6a).

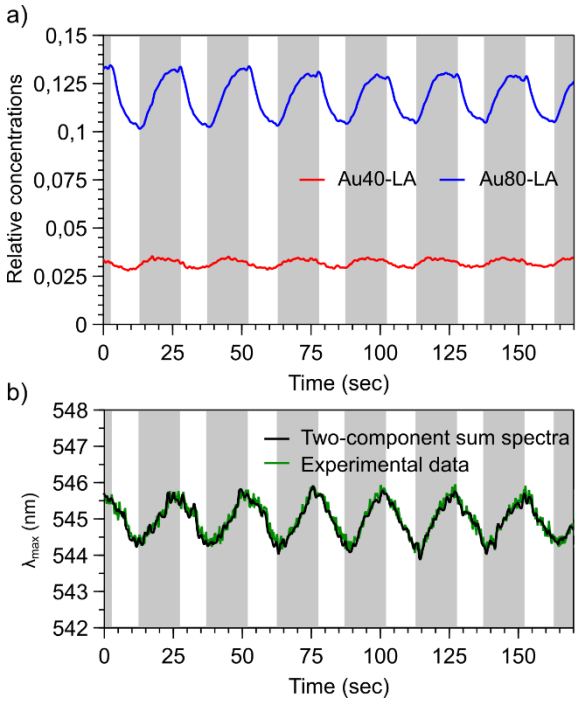

Figure 6. (a) Time-dependent variation of the relative concentrations of the individual components, Au40-LA and Au80-LA, in DEP-modulated spectroscopy, obtained through least-squares fitting of the weighted sum of the spectra of the individual components to the spectra in the spectrotemporal matrix of Figure 5. The grey areas in the background show when the DEP field was switched on. (b) Comparison of the position of the maximum (λ_{max}) of the experimental extinction spectra and the maximum of the spectra from the two-component sum using the relative concentrations from (a).

The modulation of the concentrations of the two components is clearly observable. Each component has a different modulation amplitude, and these individual amplitudes follow the trend observed for the (flow-enhanced) DEP of the individual components described above. The modulation in the spectral position of the maximum of the extinction band (λ_{max}) is fully consistent with the maxima found for the reconstructed two-component sum spectra (Figure 6b). This analysis indicates that there are no interactions between Au40-LA and Au80-LA in this solution, the extinction spectra simply being the sum of the two individual components.

This result demonstrates that it is feasible to use DEP-modulated spectroscopy to disentangle multicomponent mixtures *in-situ*. It is important to emphasize that this analysis is done on a microfluidic volume of sample and that the sample is only minimally perturbed. It is even

possible to recover the sample from the system after analysis. This demonstration of the analysis of a predefined two-component sample is deliberately simple, in order to illustrate the capability of DEP-modulated spectroscopy to perform *in-situ* multicomponent analysis. The data in the form of spectrotemporal matrices generated in these measurements is suitable for analysis using multivariate chemometric methods,[31,32] and further work is being undertaken to exploit this possibility. This is illustrated in the Supporting Information (section S7).

3. Conclusion

By employing dielectrophoresis (DEP) to periodically modulate NP concentrations in a microfluidic observation volume, optical extinction spectra of NP samples were obtained that varied over time in response to this modulation, which depends on the DEP response of the NPs. The modulation was observed to be enhanced in microfluidic flow over a linear array of DEP micro-electrode pairs by repeated capture-release at subsequent electrode pairs. The DEP-induced local concentration enhancement was relatively modest, at most a factor of 2, and did not lead to aggregation of nanoparticles, as evidenced by the absence of changes in the extinction spectra.

In this study, we first use DEP-modulated extinction spectroscopy to obtain quantitative measurements of the DEP susceptibility for gold NPs of different diameters, extending the lower limit of measurement to NPs of 40 nm diameter, and confirming the dependence of DEP susceptibility on diameter observed previously using dark-field video-microscopy.[9] Being able to characterize quantitatively the DEP response of such small NPs is important for nano-

assembly of NPs using DEP fields,[43–45] and for bioanalytical applications of NPs in combination with DEP.[46]

The second important demonstration in this work is the disentanglement of the extinction spectra of two differently sized gold NPs mixed in the same sample by DEP-modulated spectroscopy. The spectrotemporal data generated through DEP modulation of the NP concentration in the spectroscopic observation volume can be submitted to chemometric multicomponent analysis,[31,32] as demonstrated in the Supporting Information. This offers promising prospects for the *in situ* analysis of more complex NP samples, such as those encountered during the intermediate steps in the construction of DNA-programmed supercrystals.[47,48]

In its 'no flow' variation, DEP-modulated spectroscopy can function with very small (sub-microliter) volumes of NP samples. The samples can be recovered unaltered. The 'flow-enhanced' variation of DEP-modulated spectroscopy has some similarity to DEP-FFF[49,50] combined with spectroscopic detection, but it has a faster time response (seconds *vs* minutes) and is a continuous flow technique.

Starting from the results presented here, the work is now to be continued with mathematically modelling the combined microfluidic and DEP transport phenomena in order to describe precisely the time- and position-dependence of the DEP-modulation process in order to further extract hydrodynamic and electrokinetic NP properties from the measurements. Moreover, the DEP-modulated spectroscopy can be combined with chemometric methods for the characterization of more complex multicomponent particle systems. By changing the

configuration of the microscope-spectrometer combination, DEP modulation can be extended to other optical spectroscopic techniques, such as fluorescence spectroscopy or Raman spectroscopy, giving access to nanoparticles without strong optical extinction bands. It might even be used with dynamic light scattering, a technique displaying difficulties with samples containing multimodal particle distributions,[51,52] or charge-detected mass spectrometry, which is capable of measuring the gigadalton mass distribution of nanoparticle samples.[53]

4. Experimental section

Gold nanoparticles: Colloidal gold nanospheres of 40, 80 and 100 nm diameter, stabilized by carboxylic acids, were obtained from BBI (Cardiff, UK) and used as the starting materials for preparing samples. These particles are referred to as Au40, Au80 and Au100, respectively. An aqueous solution of 0.2 mM sodium lipoate (NaLA) and 1 mM NaOH was prepared using racemic (±)-α-lipoic acid (LA, Sigma, 0.2 mM) and NaOH (1.2 mM) in pure water. The conductivity of this NaLA solution was determined to be 1.8×10^{-2} S m^{-1}. The colloidal Au40, Au80 and Au100 gold NPs were coated with lipoate by mixing them with the aqueous NaLA solution. Samples were centrifuged (Hettich Mikro 220R, Germany) for 30 min at 2259 x *g* for Au40, 603 x *g* for Au80 and 514 x *g* for Au100, loosely following our own recommendations for the centrifugal acceleration.[54] Ten milliliters of each NP solution were distributed over 10 individual 1 mL centrifuge tubes and centrifuged. The supernatant was removed and the pellets of the individual centrifuge tubes were pooled in order to concentrate the particles. Then, further centrifugation cycles were performed. After each centrifugation step, the supernatant was removed and replaced (90% of the volume) by the aqueous NaLA-NaOH solution. This centrifugation-redispersion was repeated two times and the particles were finally dispersed in a

total volume of 500 µL aqueous solution (0.2 mM NaLA, 1 mM NaOH), with a NP concentration which is 25 times the initial NP concentration. The resulting solutions of lipoate-coated gold NPs are referred to Au40-LA, Au80-LA and Au100-LA. The samples were characterized using optical extinction (UV-visible) spectroscopy, confirming their integrity and providing reference spectra for the extinction spectroscopy in the microfluidic system. On basis of the extinction spectra, the concentrations of NPs in the stock solutions were determined to be 1.93 x 10^{12} particles mL^{-1} (3.20 x 10^{-9} mol L^{-1}) for Au40, 2.32 x 10^{11} particles mL^{-1} (3.85 x 10^{-10} mol L^{-1}) for Au80 and 8.95 x 10^{10} particles mL^{-1} (1.49 x 10^{-10} mol L^{-1}) for Au100. [55]

Microfluidic system: Polydimethylsiloxane (PDMS Sylgard 184 - Dow Corning) was chosen as the material for the body of the microfluidic chip. A 10:1 mix of PDMS and its cross-linking agent was degassed under reduced pressure (1 hour, 0.1 bar) and then poured on top of the photolithographically structured SU-8 mold in a Petri dish. The Petri dish containing the mold and the PDMS was cured for one hour at 70°C before the PDMS was peeled off the mold. The PDMS slabs were then cut, and inlets/outlets were punched in the PDMS. The PDMS slabs were not fixed to the substrate with plasma bonding but simply laid out over substrate, relying on the native adhesion of cross-linked PDMS to clean glass. This adhesion is strong enough to sustain microfluidic flow at low pressure without leakage, yet weak enough to be reversible, enabling cleaning and reuse of the thin-film electrode substrates. In this work, the microfluidic system consisted of a simple channel of rectangular cross-section with a height of 20 µm, a width of 300 µm and a length of 1.9 cm. The substrate was a 170 µm thick fused silica glass, carrying thin-film ITO electrodes as used previously.[9] The microfluidic circuit was operated using pressure-driven flow. A Fluigent MFCS-EZ microfluidic flow controller was used to increase the pressure precisely at the input of the channel. The output of the device was left at atmospheric pressure. The accessible pressure range is 0 to 69 mbar (above atmospheric

pressure). This corresponds to accessible flow rates of 0 to 44 μL min^{-1} on basis of the channel geometry.[56]

Extinction micro-spectroscopy: The microfluidic volume inside the device was observed through an Olympus IX71 inverted microscope using a moderate magnification objective (20x, N.A. = 0.4) using bright-field transmitted light contrast. The light source was provided by the illumination optics of the microscope (halogen light source, Osram HLX 100 W). The beam-splitter in the microscope's observation path was used to send 20% of the light onto a digital camera (Ximea xIQ-MQ013CG-ON) attached to the microscope front port (replacing the binoculars) and 80% to the optical fiber (50 μm core diameter) positioned at the side port. The optical fiber was connected to a diode-array UV-visible-NIR spectrograph (OceanOptics USB4000-VIS-NIR). Spectra were recorded using 250 milliseconds of exposure time. The useful spectral range was 430…700 nm, limited at short wavelengths by the weak blue-UV emission of the halogen lamp, and at long wavelengths by the infrared filter firmly integrated in the microscope illumination optics. This spectral range is sufficient for observing the extinction band of spherical gold NPs.

Optical spectroscopy measurements were carried out at ambient temperature on aqueous gold NP solution injected directly into the microfluidic channel. Optical extinction spectroscopy was done by first recording the dark spectrum $I_{dark}(\lambda)$, *i.e.* the spectrum recorded by the spectrometer without any light. Subsequently, a baseline spectrum $I_0(\lambda)$ was recorded by filling the microfluidic channel with water. With these spectra in place, the extinction spectrum $OD(\lambda)$ is calculated in the usual manner from the transmitted light spectrum $I(\lambda)$ recorded through the solution containing NPs.

$$\mathrm{OD} = \log_{10}\left(\frac{I - I_{\mathrm{dark}}}{I_0 - I_{\mathrm{dark}}}\right) \quad (3)$$

Multi-component analysis: For analysis of the DEP-modulation of the mixture of Au40-LA and Au80-LA inside the microchannel, spectrotemporal data obtained from the spectrophotometer were processed using a simple numerical procedure. This consists in summing the relative contributions of the single component reference spectra of Au40-LA and Au80-LA (respectively $OD_{40}(\lambda)$ and $OD_{80}(\lambda)$) using individual weighting factors k_{40} and k_{80}, respectively. The factors k_{40} and k_{80} were optimized for each time step of the DEP modulation, such that the weighted sum of the spectra (Equation. 4) best fits the spectrum of the mix solution. This was done by minimizing the error using the Nelder-Mead method.

$$\mathrm{OD}(\lambda) = k_{40}\mathrm{OD}_{40}(\lambda) + k_{80}\mathrm{OD}_{80}(\lambda) \quad (4)$$

A further check of good agreement between the fitted sum spectra and the spectra in the recorded spectrotemporal matrix was found in the fact that there is very good agreement in the wavelengths of the extinction maxima between the sum spectra and the experimental spectra.

Supporting Information

Supporting Information is available from the Wiley Online Library or from the author.

Acknowledgments

This work was supported through a Ph.D. fellowship funded jointly by ENS Rennes and *Région Bretagne* (ARED programme). Additional funding from the Institut d'Alembert (Cachan, France, project "CAFEMICRO") is gratefully acknowledged.

Conflict of interest

The authors declare that there are no conflicts of interest.

References

[1] R. L. Berger, B. Balko, W. Borcherdt, W. Friauf, *Rev. Sci. Instrum.* **1968**, *39*, 486.
[2] B. Tonomura, H. Nakatani, M. Ohnishi, J. Yamaguchi-Ito, K. Hiromi, *Anal. Biochem.* **1978**, *84*, 370.
[3] G. Porter, M. R. Topp, *Proc. Math. Phys. Eng. Sci.* **1970**, *315*, 163.
[4] W. D. Hoff, I. H. van Stokkum, H. J. van Ramesdonk, M. E. van Brederode, A. M. Brouwer, J. C. Fitch, T. E. Meyer, R. van Grondelle, K. J. Hellingwerf, *Biophys J.* **1994**, *67*, 1691.
[5] G. Boschloo, A. Hagfeldt, *Inorg. Chim. Acta* **2008**, *361*, 729.
[6] M. L. Plenert, J. B. Shear, *Proc. Natl. Acad. Sci. U.S.A.* **2003**, *100*, 3853.
[7] C. Peters, L. Wolff, S. Haase, J. Thien, T. Brands, H.-J. Koß, A. Bardow, *Lab Chip* **2017**, *17*, 2768.
[8] K. Khoshmanesh, C. Zhang, F. J. Tovar-Lopez, S. Nahavandi, S. Baratchi, K. Kalantar-Zadeh, A. Mitchell, *Electrophoresis* **2009**, *30*, 3707.
[9] C. Midelet, B. Le Pioufle, M. H. V. Werts, *ChemPhysChem* **2019**, *20*, 3354.
[10] S.-H. Liao, I.-F. Cheng, H.-C. Chang, *Microfluid Nanofluidics* **2012**, *12*, 201.
[11] H. Morgan, N. G. Green, *AC Electrokinetics: Colloids and Nanoparticles*, Research Studies Press, Baldock, **2003**.
[12] G. R. Pesch, F. Du, *Electrophoresis* **2020**, https://doi.org/10.1002/elps.202000137
[13] J. A. R. Price, J. P. H. Burt, R. Pethig, *Biochim. Biophys. Acta* **1988**, *964*, 221.
[14] R. Pethig, *Crit. Rev. Biotechnol.* **1996**, *16*, 331.
[15] T. P. Hunt, R. M. Westervelt, *Biomed. Microdev.* **2006**, *8*, 227.
[16] K.-T. Liao, C.-F. Chou, *J. Am. Chem. Soc.* **2012**, *134*, 8742.
[17] A. Nakano, A. Ros, *Electrophoresis* **2013**, *34*, 1085.
[18] L. Lesser-Rojas, P. Ebbinghaus, G. Vasan, M.-L. Chu, A. Erbe, C.-F. Chou, *Nano Lett.* **2014**, *14*, 2242.
[19] A. Rohani, B. J. Sanghavi, A. Salahi, K.-T. Liao, C.-F. Chou, N. S. Swami, *Nanoscale* **2017**, *9*, 12124.
[20] L. Velmanickam, M. Fondakowski, I. T. Lima, D. Nawarathna, *Biomicrofluidics* **2017**, *11*, 044115.
[21] N. Swami, C.-F. Chou, V. Ramamurthy, V. Chaurey, *Lab Chip* **2009**, *9*, 3212.
[22] I.-F. Cheng, S. Senapati, X. Cheng, S. Basuray, H.-C. Chang, H.-C. Chang, *Lab Chip* **2010**, *10*, 828.
[23] L. Cui, T. Zhang, H. Morgan, *J. Micromech. Microeng.* **2002**, *12*, 7.
[24] H.-Y. Lin, C.-H. Huang, W.-H. Hsieh, L.-H. Liu, Y.-C. Lin, C.-C. Chu, S.-T. Wang, I.-T. Kuo, L.-K. Chau, C.-Y. Yang, *Small* **2014**, *10*, 4700.
[25] M. Kamata, Y. Taguchi, Y. Nagasaka, *Opt. Express* **2018**, *26*, 16970.
[26] D. J. Bakewell, H. Morgan, *IEEE Trans. Nanobioscience* **2006**, *5*, 139.
[27] J. P. H. Burt, T. A. K. Al-Ameen, R. Pethig, *J. Phys. E* **1989**, *22*, 952.
[28] D. Holmes, H. Morgan, N. G. Green, *Biosens. Bioelectron.* **2006**, *21*, 1621.
[29] A. F. Chrimes, A. A. Kayani, K. Khoshmanesh, P. R. Stoddart, P. Mulvaney, A. Mitchell, K. Kalantar-Zadeh, *Lab Chip* **2011**, *11*, 921.

[30] F. G. Halaka, *Proc. Natl. Acad. Sci. U.S.A.* **2003**, *100*, 10164.
[31] C. Ruckebusch, M. Sliwa, P. Pernot, A. de Juan, R. Tauler, *J. Photochem. Photobiol. C* **2012**, *13*, 1.
[32] M. El Rakwe, D. N. Rutledge, G. Moutiers, J.-B. Sirven, *J. Chemom.* **2017**, *31*, e2869.
[33] H. Watarai, T. Sakamoto, S. Tsukahara, *Langmuir* **1997**, *13*, 2417.
[34] P. V. Jones, G. L. Salmon, A. Ros, *Anal. Chem.* **2017**, *89*, 1531.
[35] D. J. Bakewell, H. Morgan, *Meas. Sci. Technol* **2004**, *15*, 254.
[36] D. J. Bakewell, *J. Phys. D* **2011**, *44*, 085501.
[37] E. B. Cummings, A. K. Singh, *Anal. Chem.* **2003**, *75*, 4724.
[38] A. Nakano, T.-C. Chao, F. Camacho-Alanis, A. Ros, *Electrophoresis* **2011**, *32*, 2314.
[39] S. K. Ghosh, T. Pal, *Chem. Rev.* **2007**, *107*, 4797.
[40] W. Cao, M. Chern, A. M. Dennis, K. A. Brown, *Nano Lett.* **2019**, *19*, 5762.
[41] J. A. Nelder, R. Mead, *Computer J.* **1965**, *7*, 308.
[42] F. Gao, L. Han, *Comp. Optim. Appl.* **2012**, *51*, 259.
[43] P. Moutet, P. Deram, N. M. Sangeetha, L. Ressier, *J. Phys. Chem. Lett.* **2014**, *5*, 2988.
[44] K. D. Hermanson, S. O. Lumsdon, J. P. Williams, E. W. Kaler, O. D. Velev, *Science* **2001**, *294*, 1082.
[45] O. D. Velev, S. Gupta, *Adv. Mater.* **2009**, *21*, 1897.
[46] D. Kim, M. Sonker, A. Ros, *Anal. Chem.* **2019**, 277.
[47] Y. Tian, J. R. Lhermitte, L. Bai, T. Vo, H. L. Xin, H. Li, R. Li, M. Fukuto, K. G. Yager, J. S. Kahn, Y. Xiong, B. Minevich, S. K. Kumar, O. Gang, *Nat. Mater.* **2020**, 1.
[48] Y. Zhang, S. Pal, B. Srinivasan, T. Vo, S. Kumar, O. Gang, *Nat. Mater.* **2015**, *14*, 840.
[49] G. H. Markx, J. Rousselet, R. Pethig, *J. Liq. Chromatogr. Relat. Technol.* **1997**, *20*, 2857.
[50] Y. Huang, X. B. Wang, F. F. Becker, P. R. Gascoyne, *Biophys J.* **1997**, *73*, 1118.
[51] F. Destremaut, J.-B. Salmon, L. Qi, J.-P. Chapel, *Lab Chip* **2009**, *9*, 3289.
[52] L. A. Clementi, J. R. Vega, L. M. Gugliotta, *Part. Part. Syst. Charact.* **2010**, *27*, 146.
[53] M. Loumaigne, C. Midelet, T. Doussineau, P. Dugourd, R. Antoine, M. Stamboul, A. Débarre, M. H. V. Werts, *Nanoscale* **2016**, *8*, 6555.
[54] J. Midelet, A. H. El-Sagheer, T. Brown, A. G. Kanaras, M. H. V. Werts, *Part. Part. Syst. Charact.* **2017**, *34*, 1700095.
[55] J. R. G. Navarro, M. H. V. Werts, *Analyst* **2013**, *138*, 583.
[56] K. W. Oh, K. Lee, B. Ahn, E. P. Furlani, *Lab Chip* **2012**, *12*, 515.

Supporting Information

Dielectrophoretically modulated optical spectroscopy of colloidal nanoparticle solutions in microfluidic channels

Clyde Midelet[a,b] *and Martinus H. V. Werts*[a,b]*

S1. Experimental characterization of the effective observation area for microspectrocopic extinction measurements

The optical path has been kept as simple as possible in these experiments, essentially placing a fiber-coupled spectrometer at the side-port of the microscope, and adjusting it such that the circular area in the microscope image that is sampled by the spectrometer is relatively large, in order to measure an average concentration over that part of the image. The sampled area was determined experimentally by scanning the microfluidic device relative to the microscope objective using a motorized sample stage while recording the evolution of the light intensity detected by the spectrometer. The microfluidic structure contains sharp, small features of sufficient optical contrast (microfluidic channel walls, ITO microelectrodes) that serve as spatial step functions from which the spatial resolution and the diameter of the detected circular area can be determined

The evolution of the detected optical spectrum as a function of spatial position of the translation stage is shown in Figure S1a. From the microscope image of the device, a line profile (one pixel wide) was extracted and plotted to identify the position of the walls in the image and compare it to the same features recorded on the spectrometer while scanning the microfluidic device.

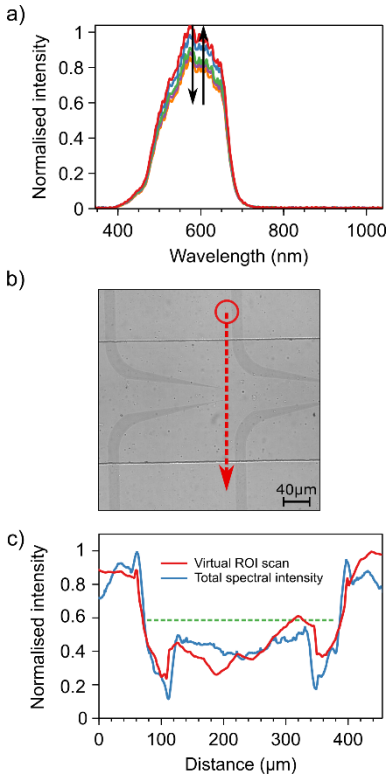

Figure S1. (a) Evolution of recorded light spectra as a function of the position of the sample. (b) Brightfield image of the microfluidic channel. The red circle shows the area swept along the red dotted line profile whose corresponds to the experimental observation and the virtual ROI scan. It was decided to avoid the crossover with electrode tips in order to minimise an extra useless intense signal between the microfluidic walls. c) Normalised intensity as a function of the distance from experimental measurement on the spectrometer (blue), and from virtually sweeping a circle (51 µm diameter) along the red dotted line profile (red).

Two correlated intensity-*vs*-position profiles were thus generated. One profile is the experimental profile of the detected spectral intensity as a function of sample position, recorded using the spectrometer while scanning the sample stage. The second is a "virtual profile" generated by numerically scanning a virtual circular region-of-interest over the microscope camera image and tracing the integrated intensity in this ROI as a function of position. The diameter of this circular ROI is adjusted such that the virtual profile (red profile) has the same shape as the experimental profile (blue profile) (see Figure S1) The experimental profile was best reproduced using an ROI diameter of 51 µm.

S2. Reference extinction spectra

Extinction spectra of the solvent baseline and of an aqueous solution containing Au40-LA nanoparticles (NPs) are shown in Figure S2. The optical path length through the sample is 20 µm. The Au40-LA particles have been prepared at a concentration of 2.75 x 10^{-9} mol L^{-1} (corresponding to an OD of 25 at 1 cm).

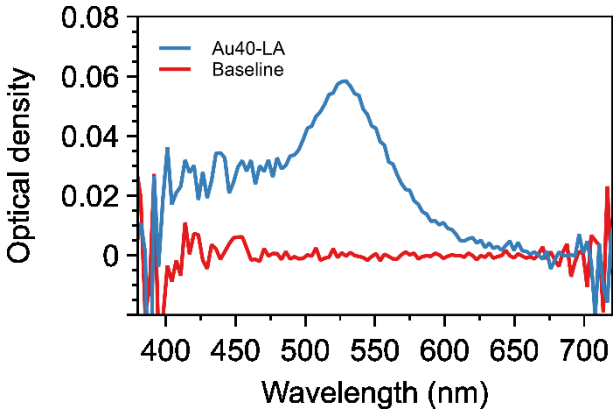

Figure S2. Baseline spectrum obtained using water injected in the microchannel (red line) and extinction spectrum of Au40-LA solution (blue curve) injected into the microchannel.

S3. DEP-modulated extinction spectra

Figure S3 contains the variations of the optical density at the wavelength of maximum extinction for the gold NPs as a function of time in the absence of microfluidic flow. In order to correct for differences in the optical densities of the injected solutions at equilibrium, the optical densities are scaled with respect to the equilibrium optical density OD_{eq}.

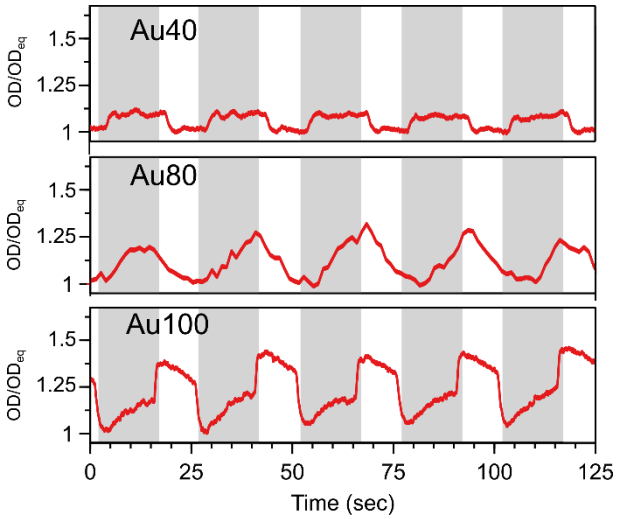

Figure S3. DEP modulation cycles of Au40-LA, Au80-LA and Au100-LA in water without microfluidic flow monitored via the relative optical density as a function of time, at the wavelengths of the extinction maximum (λ_{max} = 526 nm, λ_{max} = 549 nm, λ_{max} = 572 nm, respectively). The grey areas in the background show when the DEP field active.

S4. Flow-enhancement of DEP modulation

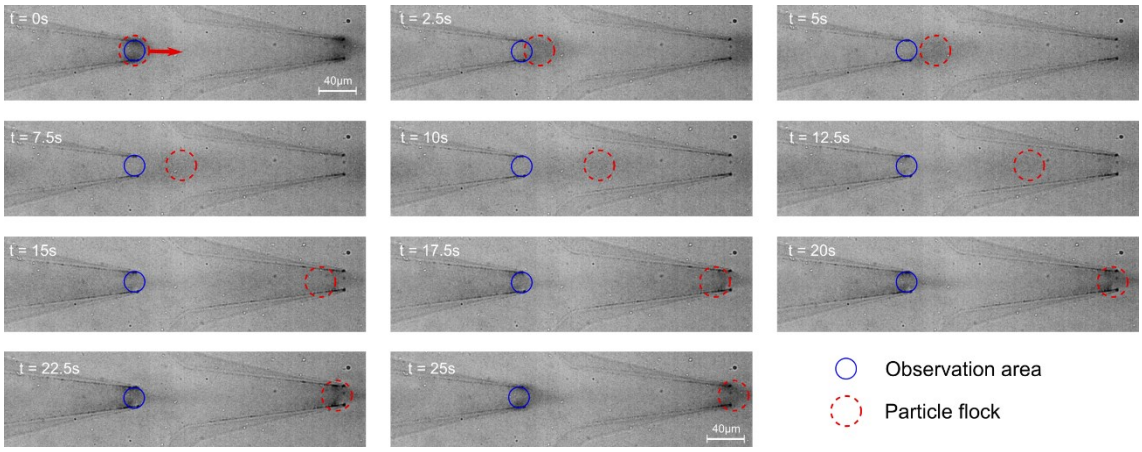

Figure S4. Mechanism of flow-enhanced DEP modulation. Selected frames from video-microscopy (transmitted-light bright-field; contrast was digitally enhanced to bring out the nanoparticle (NP) flock more clearly). The DEP "capture-and-release" cycle is repeated to capture more and more gold NPs at each electrode pair along the microchannel. The fluid flow is tuned such that a released particle "flock" arrives at the next electrodes pair when DEP is switched "ON" again. t = 0 sec corresponds to the switching "OFF" of the DEP field (release of particles).

The microfluidic flow velocity of flow-enhanced DEP is optimized as follows. Electrode pairs are separated from each other by a distance of 300 µm. In each dielectrophoresis cycle, the electric field is switched off for 10 seconds, during which they should be transported to the next electrode pair. This means that particles must be transported by the fluid at an average velocity of 30 µm s^{-1}. In our microchannel geometry, this corresponds to a fluidic pressure differential $\Delta P = 2.35$ mbar.[S1] Setting of the correct flow velocity was confirmed using dark-field particle tracking measurements, and by observing maximum flow-enhancement of the dielectrophoresis.

S5. Solutions used for studying feasibility of multicomponent analysis using DEP-modulated spectroscopy

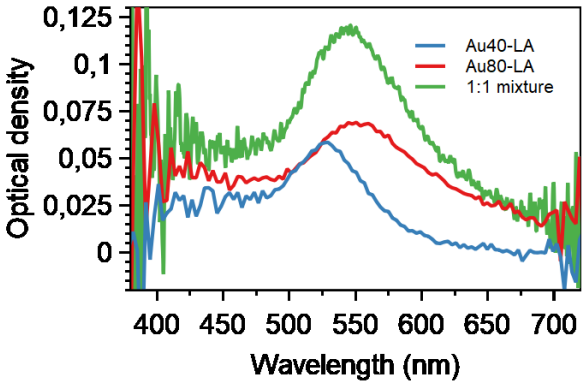

Figure S5. Spectra of stock solutions of Au40-LA, Au80-LA and a 1:1 (by volume) mixture of Au40-LA and Au80-LA solution, respectively, recorded inside the microchannel using an exposure time of 250 ms.

S6. Video of flow-enhanced DEP-modulated extinction spectroscopy

Included with this Supporting Information is a video:

`DEP-modulated_spectroscopy_simultaneous_image_and_spectrum.mp4`

It shows a recording of the microscope image of microfluidic channel with the ITO microelectrodes and injected nanoparticle solution. In parallel, it also shows the optical extinction spectrum of the sampling volume that was recorded simultaneously. The NP solution is the 1:1 mixture of Au40-LA and Au80-LA NPs also used in the multicomponent analysis demonstration. All experimental parameters were the same as those used for those measurements (AC electric potential of 1 MHz, 20 V_{pp} applied to the electrodes; DEP field active for 15 seconds ("ON"), inactive for 10 seconds ("OFF"); microfluidic flow speed of 30 $\mu m\ s^{-1}$). The included video is accelerated 5 times compared to the original recording. This acceleration was achieved by sampling only one in five frames from the original recording at constant frame rate (20 frames per second).

S7. Demonstration of chemometric analysis of spectrotemporal data matrix obtained by DEP-modulated spectroscopy

In the main text, we stated that the spectrotemporal data generated in DEP-modulated spectroscopy is amenable to analysis with chemometric methods. Here, we include a brief demonstration of the feasibility of one particular chemometric approach, based on singular value decomposition of the data matrix followed by rank reduction and transformation of the retained components to fit a specific physicochemical model of the sample's behaviour. Related approaches for analysing time-resolved spectral data have been described in the literature,[S2,S3] and fall under the general paradigm of target-transformation factor analysis (TTFA).[S4] We apply our TTFA analysis to the data presented in Figure 5, in which a mixture of gold NPs of two different diameters was measured using DEP-modulated extinction spectroscopy.

The set of m extinction spectra (optical density, OD, as a function of wavelength), each containing n OD data points, can be represented by the n x m matrix **A**. In absence of noise, each spectrum is the sum of the spectral contributions of all the (chemical/nanoparticle) species in the sample. For p individual species in the sample, we can write their specific spectral responses (*e.g.*, relative or absolute extinction coefficients) as the columns of an n x p matrix **S**. The (relative or absolute) concentrations that are evolving over time (in this work: as a result of DEP modulation) will then be in a p x m matrix **C**. The spectrotemporal matrix is the product of the spectral and concentration matrices (Eq. S1).

$$\mathbf{A} = \mathbf{SC} \qquad \text{(Eq. S1)}$$

In typical analysis cases, only **A** is known, and the objective is to find **S** and/or **C**. In the particular case of the data shown in Figure 5, we did actually have access to **S**, since we prepared a mixture ourselves from pure NP components, and in the Main Text a straightforward fitting

procedure was utilized for extracting the concentration data (Figure 6). For the sake of illustrating the chemometric analysis, we pretend here that **S** is unknown.

The first step of the analysis is singular value decomposition (SVD) of the spectrotemporal matrix. SVD is based on the fact that any n x m matrix (*e.g.*, **A**) can be decomposed into two unitary matrices, **U** and **V**, and a diagonal matrix **W** (sometimes denoted **Σ**) such that

$$\mathbf{A} = \mathbf{U}\mathbf{W}\mathbf{V}^{T} \qquad \text{(Eq. S2)}$$

The diagonal elements of **W** are called the singular values and they appear in descending order. The column vectors of **U** and **V** all have length 1. It is therefore the singular values that determine the weight of the contribution of each column vector to the total matrix. For the matrix **A**, in the absence of noise, the only non-zero singular components would be the first p components, the matrix being of rank p. With noise, there is no such extreme cut-off, but singular value decomposition still gives a good indication of the rank of the underlying ideal (noise-free) data matrix. By selecting only the first k components of the SVD, a rank-reduced representation of the data is obtained. This removes noise from the data, and also compresses the data, since a good approximation of the full n x m matrix can be reconstructed from an n x k and a k x m matrix.

An important aspect of the rank estimation provided through SVD is that it indicates how many independent chemical species (*e.g.*, different types of NPs) contribute to the measured spectra, purely on basis of the properties of the data matrix, without *a priori* chemical knowledge. Figure S6 (left) contains a graph of the singular values of the first 10 components of the SVD of the spectrotemporal data from Figure 5 (main text). Only the two first singular values stand out, and the other components show a steadily decreasing trend. This is in very good agreement with the fact that we used a sample with two different NP populations (40 nm and 80 nm diameters).

The first singular value is high compared to the second, which is likely due to the similarity of the extinction spectra of 40 nm and 80 nm gold NPs.

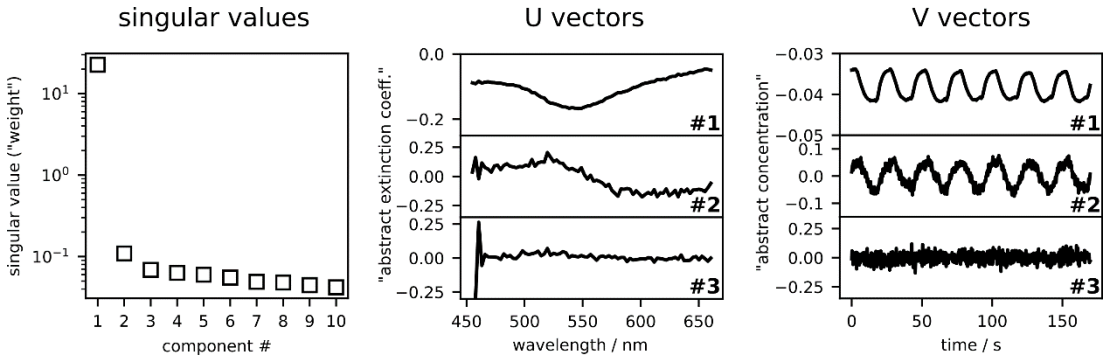

Figure S6. Graphical representation of the singular value decomposition of the DEP-modulated spectrotemporal data matrix from the experiment in Figure 5 (main text). *Left*: singular values of the first 10 components (logarithmic ordinate). *Centre*: first 3 vectors of the **U** matrix containing the spectral profile information. *Right*: first 3 vectors of the **V** matrix containing concentration-*vs*-time information.

Inspection of the column vectors of **U** and **V** (Figure S6, centre and right) shows that indeed only the first two components contain DEP-modulated spectral information. The spectrotemporal matrix **A** can be well approximated from **U**, **W** and **V**, only retaining $k = 2$ components. In order to avoid subscripts, we will simply continue writing **U**, **V** and **W** below, bearing in mind that these now refer to their rank-reduced versions of dimensions n x k, m x k, and k x k, respectively.

In Figure S6, it is furthermore seen that whereas the spectral and concentration vectors do appear to contain relevant information, they have an unphysical form (*e.g.* negative concentrations). Indeed, these vectors are linear combinations of the real physically-relevant vectors. Interestingly, they may be transformed into their physically meaningful counterparts using a k x k transformation matrix **T**. Combining Eqns S1 and S2, and inserting $\mathbf{T}^{-1}\mathbf{T}$ we find

$$\mathbf{SC} = \mathbf{U}\mathbf{T}^{-1}\mathbf{T}\mathbf{W}\mathbf{V}^{T} \qquad \text{(Eq. S3)}$$

If, for instance, we are able to find a **T** such that **V** is related to (a model of) **C**, *i.e.*

$$\mathbf{C} = \mathbf{TWV}^{T} \qquad \text{(Eq. S4)}$$

Then we will also obtain **S**, after inversion of **T**.

$$\mathbf{S} = \mathbf{UT}^{-1} \qquad \text{(Eq. S5)}$$

Further work is required to formulate and validate physicochemical models of **C**. This involves modelling the evolution of the concentrations of the NPs in the microfluidic observation volume as a function of time under DEP modulation and is part of future work. In the present case, for demonstration purposes, we use the convenient short-cut provided by the fact that we already obtained the time-evolution of the concentration of both species in **C** using the straightforward procedure in the main text (Figure 6). The four matrix elements of **T** were found using a simple Nelder-Mead optimization, iteratively re-calculating Eqn S4 until the difference between **C** and the concentration curves from Figure 6 was minimal. The result of the transformed SVD components is shown in Figure S7.

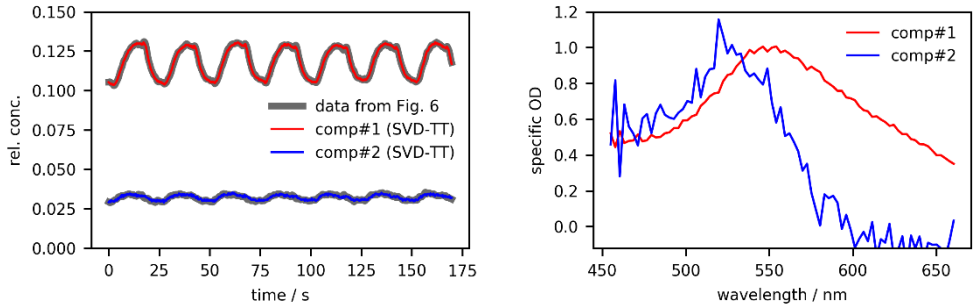

Figure S7. The two components of the rank-reduced SVD after transformation such that the concentration traces reproduce the concentration traces obtained in Figure 6 (main text). *Left*: concentration vectors (**C** = **TWV**^{T}), showing the modulation of gold NP concentration by DEP. *Right*: spectral vectors from the target-transformed SVD (**S** = **UT**$^{-1}$), agreeing with the known spectra for Au40-LA and Au80-LA NPs.

The transformation indeed yields modulated concentration traces that closely fit the concentration traces obtained in the main text. Additionally, the corresponding 'pure species' spectra of both components are recovered automatically, and are close to the spectra of the 40

nm and 80 nm gold particles that were put into the mixture. This demonstrates the feasibility of chemometric analysis of DEP-modulated spectroscopy data for gold NPs, and opens the possibility of studying more complex samples of only partially known composition using DEP-modulated spectroscopy.

References

[S1] K. W. Oh, K. Lee, B. Ahn, E. P. Furlani, *Lab Chip* **2012**, *12*, 515.

[S2] M. Koeberg, M. H. V. Werts, H. J. van Ramesdonk, J. W. Verhoeven, *EPA Newsletter* **2001**, *71*, 21.

[S3] L. Zimanyi, A. Kulcsar, J. K. Lanyi, D. F. Sears, J. Saltiel, *Proc. Natl. Acad. Sci. U.S.A.* **1999**, 4408.

[S4] P. J. Gemperline, *Anal. Chem.* **1986**, *58*, 2656.